ACS APPLIED NANO MATERIALS

www.acsanm.org Article

Monolayer Graphene Grown on Nanoscale Pt Films Deposited on TiO_2 Substrates for Micro- and Nanoelectromechanical Systems

Joon Hyong Cho,[‖] Yoonho Seo,[‖] Andrei Dolocan, Neal A. Hall, and Michael A. Cullinan*

Cite This: *ACS Appl. Nano Mater.* 2020, 3, 9731−9739 Read Online

ACCESS | Metrics & More | Article Recommendations | Supporting Information

ABSTRACT: This study presents chemical vapor deposition (CVD) growth of high-quality monolayer graphene on 100 nm-thick Pt thin films deposited on TiO_2-coated silicon wafers. Conventional graphene growth on Pt thin films using CVD requires relatively thick films because of potential dewetting issues, which limits fabrication integration for nano-/microelectromechanical system (NEMS/MEMS) devices. Additional metal interlayers are commonly introduced to provide good adhesion between the Pt thin film and the substrate to achieve reliable graphene growth on thinner thin films. However, growing high-quality graphene on the Pt films with a thickness of less than 100 nm has still not been demonstrated because of dewetting issues. In this work, we introduce TiO_2 as an adhesion layer for Pt on a Si substrate for graphene growth and show that using this adhesion layer, we are able to achieve large-area coverage of high-quality graphene without significant surface dewetting of a 100 nm Pt thin-film substrate. These results are confirmed by time-of-flight secondary ion mass spectrometry and Raman spectroscopy measurements. Our results show that graphene growth on Pt thin films can be more reliable using TiO_2 as an adhesion layer and provides a guide for integration of growth of graphene onto the NEMS/MEMS device during the fabrication process.

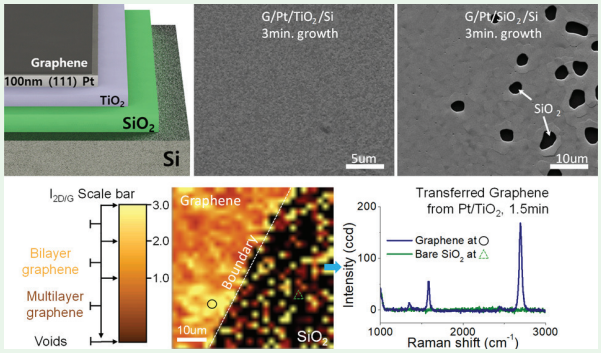

KEYWORDS: *graphene, chemical vapor deposition (CVD), platinum, thin film, solid-state dewetting*

1. INTRODUCTION

Graphene is a two-dimensional (2D) honeycomb lattice structure of sp^2-bonded carbon atoms and has been known for its exceptional material properties for more than a decade. Yet understanding graphene's growth mechanism along with finding an appropriate growth substrate has been a significant problem,[1−5] especially for device applications in nano-/microelectromechanical systems (NEMS/MEMS). In order to successfully produce high-quality monolayer graphene on a metal catalyst with high reliability, repeatability, and at a large-scale, many experimental growth parameters must be evaluated.[6,7] One of the most challenging decisions is choosing a robust metal catalyst on the growth substrate which provides the foundation for graphene growth. Previously, graphene growths on Ru, Ir, Pt, Ni, and Cu have been conducted, and electrical properties along with other properties of graphene have been analyzed.[6,8−14] The graphene growth mechanism using chemical vapor deposition (CVD) is different on different transition metals because of the different solubility of carbon atoms in these metals.[6,15]

Pt has been a material of choice for a wide range of MEMS applications because of its excellent properties, such as high chemical inertness, high resistance to oxidation, and its integration feasibility into complementary metal−oxide−semiconductor and existing Si-based micromachining processes.[16] Pt has particularly gained much attention in the high-quality graphene growth owing to many benefits over other counterparts of Ni and Cu such as lower surface roughness and high thermal stability.[16−20] In addition, Pt leaves no residue on the graphene layer during the growth and transfer process to other substrates, as would be the issue in Cu.[21,22] With moderate carbon solubility (between that of Cu and Ni), Pt allows a sufficient process window for the monolayer graphene.[15] The coefficient of thermal expansion difference between Pt and graphene is also much smaller than other common growth catalysts such as Cu and Ni. This is another advantage for Pt as a growth catalyst because the thermally induced stress is proportional to the coefficient mismatch between the materials, and high thermal stresses result in the degradation of the subsequent graphene layer.[23−25] As an example, highly (111)-oriented Pt has recently been demonstrated as an excellent catalyst for the high-quality monolayer graphene growth.[16,26,27]

Received: July 7, 2020
Accepted: September 9, 2020
Published: September 9, 2020

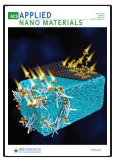

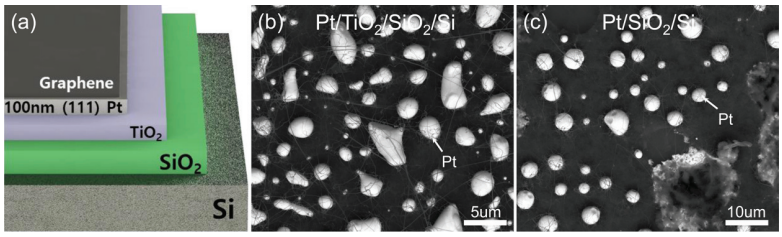

Figure 1. (a) Ideal layer composition of graphene on top of 100 nm (111) Pt, TiO_2, SiO_2, and Si substrates. Dewet surface after excessive time of graphene growth on 100 nm Pt thin film on (b) $TiO_2/SiO_2/Si$ substrate and on (c) SiO_2/Si substrate at 1030 °C for 30 min.

Previously, graphene growth on Pt foil was conducted using the fast cooling method,[28] and it was able to selectively grow monolayer graphene. Furthermore, an electrochemical delamination technique introduced a new way of transferring graphene onto different substrates, hence eliminating the need for etching Pt foil to transfer graphene and enabling the reuse of the foil for the subsequent graphene growth.[29] However, this transfer technique is not ideal because it requires manual handling of graphene composite layers. In other words, any graphene devices that are designed for mass production cannot be automated via conventional transfer of graphene. In addition, conventional transfer of graphene approach is not cost-effective and can cause yield and repeatability problems of fabricating graphene devices. Therefore, graphene growth on NEMS/MEMS devices becomes more feasible by adapting graphene growth on Pt thin films which support mass production and yield improvements. Lithography-friendly fabrication of graphene has been proposed[30] in which a thin metal film is used in place of the foil to integrate graphene growth process as a part of MEMS device fabrication. However, there are still issues with using metal thin films for high temperature of graphene growth. For example, depositing thicker metal films is favorable for the better thermal stability of the layer, but deposition of thick films (>1 μm) is not cost- and time-effective, especially when Pt is used over Ni or Cu thin films. Also, controlling monolayer graphene growth is not trivial as the thin film gets thicker. It has been reported that multilayers can be grown on thicker thin films when the film is deposited on the adhesion layer.[31]

Another challenge with growth of graphene on Pt thin films is that Pt has poor adhesion property on top of SiO_2/Si substrates. The lack of an adhesion layer causes Pt thin film to experience a large degree of agglomeration (i.e., solid-state dewetting[19]) or film delamination during graphene growth at high temperature, which threatens the yield of graphene production. As an effort to address such issues resulting from Pt adhesion, Ti has been favorably employed as an intermediate adhesion layer. However, Ti still has posed diffusion-related issues at high temperatures, such as Pt hillock formation or TiO_x formation in and on Pt, threatening the quality of subsequent layer growth and in turn, the device performance.[32−35] In addition, potentially better candidates of adhesion layers were discussed previously where it was found that adhesion layers that favor graphene growth when alloyed with Pt[15] induce better quality of graphene.

TiO_2 has recently been introduced for Pt adhesion instead of Ti[36,37] in ferroelectric device applications. The use of TiO_2 addresses the diffusion-related issues present in Ti while retaining moderate Pt adhesion and high degree of (111)-Pt orientation, leading to improved thermal stability and in turn, ferroelectric devices with high performance and reliability.[38,39] Considering these aspects, highly (111)-oriented Pt thin film with TiO_2 adhesion layer is anticipated as a promising substrate for the high-quality monolayer graphene growth. Despite the merits discussed above, Pt thin film deposited on a TiO_2 adhesion layer has not gained much attention for graphene growth.

In this study, we present Pt thin film with a TiO_2 adhesion layer for the monolayer graphene growth. Pt thin films with and without the TiO_2 layer are prepared for graphene growth and compared against each other. Significant improvement in Pt agglomeration has been noted in Pt film with the TiO_2 layer with a high degree of (111)-Pt orientation retained after graphene growth. Monolayer graphene growth has been successfully demonstrated and confirmed by Raman and time-of-flight secondary ion mass spectrometry (TOF-SIMS) measurements.

2. BACKGROUND

2.1. Background on Dewetting in Thin Film. Surface dewetting is a phenomenon which acts to reduce the free surface energy of the film interface. Graphene growth temperature at 1000 °C provides enough energy for Pt atoms to gain mobility to agglomerate on the surface. While Pt atoms are mobile, the thin metal film will rearrange so that it minimizes the total surface energy of the film. If sufficient energy is provided to the thin film, the film will form tiny ball-shaped islands, and spaces between these islands will remain vacant. According to Young's equation below ,[40] this phenomenon can be accelerated by thinner films (t, thickness) and the wetting angle between Pt thin film and the underlying substrate (θ, wetting angle). R corresponds to the average radius of grain sizes of Pt thin film.

$$\left(\frac{R}{t}\right) > \frac{3\sin^2\theta}{2 - 3\cos\theta + \cos^3\theta}$$

This phenomenon is critical for graphene growth because graphene only grows on top of the thin film and will be discontinuous on metal-vacant spaces. As dewetting gets dominant on the surface, less surface area will be available for graphene growth. In addition, when dewetting occurs, the surface morphology changes abruptly, causing fragmentation of the graphene growth because of different height profiles on the surface. An example of a dewet surface of a Pt thin film due to extensive heat source is shown as compared to ideal composition of graphene on Pt thin film on TiO_2, SiO_2, and Si substrates in Figure 1a−c. To effectively prevent the dewetting, thicker films or an increasing average radius of grain size can be used. However, increasing the radius of grain size is generally achieved by annealing the thin film at high temperatures for long periods of time, which can also potentially cause dewetting for graphene growth. In addition,

https://dx.doi.org/10.1021/acsanm.0c01839
ACS Appl. Nano Mater. 2020, 3, 9731−9739

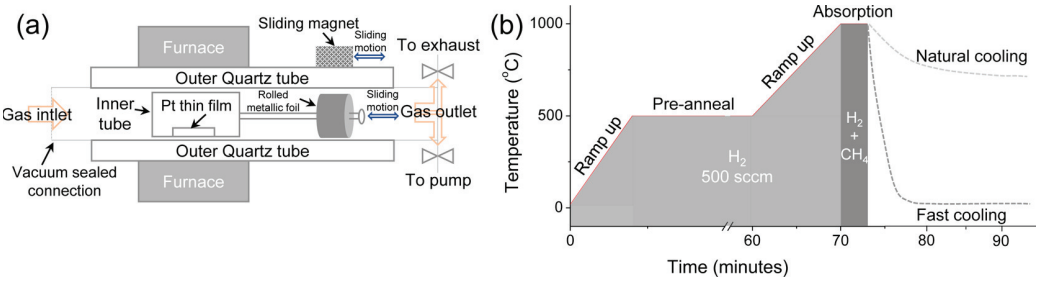

Figure 2. (a) Schematic view of the APCVD system. (b) Graphene growth process according to temperature versus time in minutes with different gas flowing sequences.

depositing thicker thin film requires extra overall time and cost for fabrication processing. Previously, it has been discussed that enabling graphene growth on thin film is a critical process for integrating graphene into the conventional NEMS/MEMS fabrication process.[7,30] The biggest challenge here is finding the cost-effective thin film deposition process which further enables reliable graphene growth on thinner Pt thin films.

2.2. Use of Adhesion Layers in Thin Films for Graphene Growth. Introducing an adhesion layer between Pt thin film and the substrate is one way to increase the reliability of the substrate during graphene growth at high temperature. Graphene growth with and without various adhesion layers on Pt thin film have been reported previously,[15,27] which showed significant improvement of thermal stability of the substrate, depending on the intrinsic material property of the adhesion layer. In addition, alloying property between Pt thin film and the adhesion layer plays an important role characterizing the quality of graphene grown on the substrate[15,31] because graphene growth temperature provides sufficient energy for two thin film metals to diffuse to one another. However, the adhesion layer itself has constraints on thermal stability, even though it is alloyed to the Pt thin film during graphene growth. Pt is thermally stable compared to majority of adhesion layers discussed previously;[15] however, the adhesion layer still can be the limiting factor of the cause of dewetting on graphene growth at high temperature. Unlike metal adhesion layers, TiO_2 has been known as a reliable adhesion layer, as shown by its application in ferroelectric devices and ease of deposition on the SiO_2/Si substrate.[36,37] In addition, diffusion between Pt thin film and TiO_2 is minimized compared to Pt thin film and other metal adhesion layers. Therefore, we find the TiO_2 layer as the best adhesion layer available for Pt thin film on the SiO_2/Si substrate reported so far because of its thermal stability and NEMS/MEMS fabrication compatibility.

3. EXPERIMENTAL SECTION

3.1. (111) Pt Film Preparation. (111)-oriented Pt thin films are deposited on $TiO_2/SiO_2/Si$ and SiO_2/Si substrates. The two samples are prepared in order to: (i) study the effect of the TiO_2 adhesion layer on thermal stability of Pt film during graphene growth, (ii) quantify the remaining area of graphene on top of each surviving Pt thin film, and (iii) compare the quality of the graphene monolayer grown on both substrates. A (100)-oriented 4 in. Si wafer is piranha-cleaned and thermally oxidized to grow 300 nm-thick SiO_2. Then, 20 nm thick (0002)-oriented Ti is deposited on SiO_2 using a sputtering system (Univex 450B, Oerlikon Leybold Vacuum Inc.), followed by thermal oxidation to form 30 nm-thick (200)-oriented TiO_2 at 750 °C for 3 h using a furnace. 100 nm-thick Pt is then deposited on the TiO_2 substrate at 500 °C using a sputtering system (Custom model, Kurt J. Lesker Company Ltd.). Fox et al. present that 30 nm-thick (200)-oriented TiO_2 is optimum for the highest (111)-Pt crystallinity;[41] therefore, this TiO_2 thickness is chosen for this study. Thickness of Pt can be determined by considering a trade-off relationship between the material-associated cost and high thermal stability. The 100 nm-thick Pt layer is one of the thinnest films reported to be thermally stable and has been widely used in graphene-integrated device applications.[15,27]

3.2. (111) Pt Film Characterization. X-ray diffraction (XRD) measurement was performed to study the effect of graphene growth on (111)-Pt orientation using an XRD instrument (Rigaku SmartLab, Rigaku Corp.). The actual positions in ω and 2θ were calibrated against those of a (400)-Si reference peaks owing to the single crystal and known 2θ position with high precision. $\omega-2\theta$ XRD measurement was then performed over the range of 2θ from 30 to 90°, where Pt peaks of interest are fully captured, with a scan speed and scan step equal to 2°/min and 0.02°, respectively. Full width at half maximum (FWHM) was computed using a software in the XRD instrument. The XRD data were normalized to their relative reference peak intensity for sample-to-sample comparison.

Scanning electron microscopy (SEM) measurements were performed to visualize the dewet surface of the Pt thin film using FEI Quanta 600 ESEM at 20 kV. Because of the roughness of the Pt thin film and the atomic thickness of the graphene layer, graphene was not visible and only the morphology of the Pt thin film was observed. Graphene grown on each $Pt/TiO_2/SiO_2$ and Pt/SiO_2 substrates with 1.5 and 3 min growth time was analyzed with SEM images.

3.3. Graphene Growth on (111)-Oriented Pt Film. Graphene growth was done under a conventional atmospheric pressure chemical vapor deposition (APCVD) furnace system, which is composed of inlet gas flow controllers, heating furnace, quartz tubes, a mechanical pump, and an outlet gas divider, as shown in Figure 2a. Two quartz tubes were used where the outer tube had a diameter of 2.54 cm. The 2 cm-diameter inner quartz tube was used to hold the Pt thin film substrate and could be moved in and out of the heat zone inside the furnace using a magnet and metallic foil wrapped around the end of the inner quartz tube. Therefore, inner tube was isolated from the atmosphere but was movable across different heat zones of the furnace. This setup made it possible to reduce the cooling time of the sample and minimize the dewetting of the Pt thin film. In addition, fast cooling has previously been exercised for effectively growing monolayer graphene growth on Pt thin films.[28]

To start graphene growth, the outer quartz tube is vacuumed with a mechanical pump to reach a stable pressure at 30 mTorr. Then, the carrier gas of 300 sccm of argon (Ar) and 100 sccm of hydrogen (H_2) are flown into the tube, and the temperature of the furnace is ramped up to 300 °C. The system is held at 300 °C for 30 min. After brief annealing, the mechanical pump valve is shut to fill the outer tube with gases until atmospheric pressure is reached. Once the outer tube pressure is above atmospheric pressure, the outlet valve to atmospheric gas exhaust is open. Furnace temperature is set to 1000 °C, and once it reaches the temperature, 20 sccm of methane (CH_4) is flown into the system to start graphene growth. Different graphene growth times are used for each run. We have tested three different growth times (1.5, 3, and 5 min) to determine the degree of dewetting and the graphene quality for each of the Pt thin films

https://dx.doi.org/10.1021/acsanm.0c01839
ACS Appl. Nano Mater. 2020, 3, 9731−9739

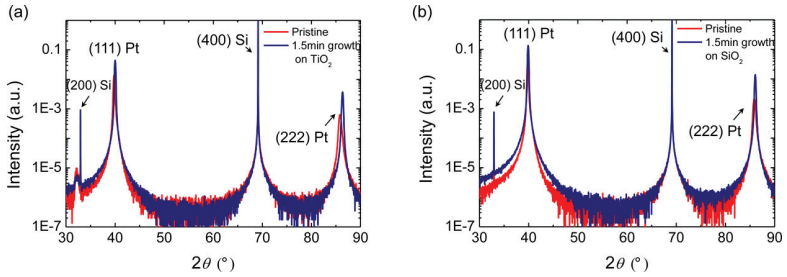

Figure 3. XRD analysis of Pt deposited on (a) TiO_2 and (b) SiO_2 substrates, respectively. Each graph shows before/after growth analysis of XRD.

deposited on TiO_2/Si and SiO_2/Si substrates. Graphene growth recipe is visualized in Figure 2b. After the growth time, the inner quartz tube holding graphene grown on Pt thin film is pulled out of the heat zone of the furnace using a magnet located outside the tube and allowed to cool for 60 min. The graphene grown-Pt thin film samples are then retrieved from the system and characterized.

3.4. Graphene Characterization. The graphene samples grown on Pt/SiO_2 and Pt/TiO_2/SiO_2 substrates for 1.5, 3, or 5 min are analyzed first with TOF-SIMS. TOF-SIMS depth profiling was performed on graphene on the Pt thin film sample, with data acquired in both positive and negative polarities to completely map the chemical content of the films. A Cs^+ sputtering ion beam (500 eV ion energy, ~40 nA measured sample current, raster scanning 300 × 300 μm^2 areas) was used to sequentially ablate the surface of the sample, while a Bi_3^+ polyatomic ion beam (30 keV ion energy, ~3 pA measured sample current, raster scanning 100 × 100 μm^2 areas centered within the Cs^+ sputtered areas) was used to analyze the regressing surface. Several species of interest were detected, among which we selected a large secondary ion carbon fragment, C_9^-, as a graphene marker (see Supporting Information). We specifically used a Bi_3^+ polyatomic analysis ion beam to enhance the yield of large secondary ion fragments.[42,43] To compare the graphene layers quantitatively between samples, we looked at the integral of the C_9^- depth profiles (i.e., the total C_9^- count) in the first 12.5 s of Cs^+ sputtering positive polarity, which provided the depth profile distribution of the Pt thin film along with the underlying adhesion layer Ti and the substrates TiO_2 and SiO_2.

Because graphene on the Pt thin film exhibits strong fluorescence using a Witec Micro-Raman Spectrometer Alpha 300 (λ = 488 nm), we transferred each grown graphene onto separate SiO_2/Si wafers for Raman inspection. Graphene samples were spin-coated with polyvinylidene fluoride (PVDF) and annealed to strengthen the bonds between the polymer chains. PVDF on the edge side was partially removed using acetone so that the Pt thin film can be effectively etched in aqua regia solution which is a mixture of nitric acid and hydrochloric acid in 1:3 ratio. The etching solution is also diluted with deionized water to slow down the etching rate. Once the Pt thin film is fully etched, PVDF/G film is transferred onto a separate clean SiO_2/Si substrate. In order to increase adhesion between graphene and the SiO_2/Si substrate, the sample is annealed at 120 °C for 60 min. Finally, PVDF is removed using a combination of heated acetone and *N*-methylformamide for several hours. Small area (10−50 μm^2) mapping of Raman spectroscopy is done on graphene on SiO_2/Si to measure and analyze the intensity of Raman peaks in range of 1000−3000 cm^{-1}.

4. RESULTS AND DISCUSSION

4.1. Effect of Graphene Growth Temperature on the (111) Pt Orientation. Highly (111)-oriented Pt thin film is a critical requirement for high-quality monolayer graphene on Pt[26] and is known to favor weak coupling between graphene and the Pt substrate. Two samples of Pt films on TiO_2 and SiO_2 substrates were prepared to study the effect of graphene growth on the (111)-Pt orientation. Figure 3 presents XRD data for both Pt samples before and after graphene growth, with details regarding the normalized intensity and FWHM of (111)-Pt peaks, as summarized in Table 1. The intensity and

Table 1. FWHM and Normalized Intensity of (111)-Pt Peaks in Pt/TiO_2/SiO_2/Si and Pt/SiO_2/Si Samples

	(111)-Pt peak in Pt/TiO_2 sample:		(111)-Pt peak in Pt/SiO_2 sample:	
graphene growth time (min)	FWHM (deg)	normalized intensity	FWHM (deg)	normalized intensity
0	0.304	0.014	0.270	0.037
1.5	0.228	0.043	0.224	0.135

FWHM of (111)-Pt peak in both samples closely resemble each other before graphene growth, indicating comparable (111)-Pt crystallization is achieved. Comparing XRD data with those reported by others demonstrated a high degree of (111)-Pt orientation in both Pt samples.[39] A slightly lower intensity and wider FWHM of the (111)-Pt peak in the Pt/TiO_2 sample is noted, which can be attributed to the TiO_2 film as its crystalline orientation [rutile (200)-orientation] also affects the (111)-Pt orientation.[36,41] After graphene growth, both samples retain their (111)-Pt peaks with a small change in FWHM, indicating the (111)-oriented Pt surface is well-retained (see Table 1). The small change is associated with thermal-annealing effect imposed by the graphene growth. In addition, other Pt peaks, such as [(200)- and (311)-Pt peaks], are not present after the graphene growth.

4.2. Effect of Growth Time on Morphology of the Substrate. For each graphene growth run, both the Pt/TiO_2/SiO_2 and Pt/SiO_2 substrates are loaded into the inner quartz tube simultaneously, as shown in Figure 4a. Because each set of sample is run at the same growth times and conditions, each run has the same amount of heat exposed to both samples. Figure 4b shows the amount of dewetting for each Pt sample as a function of growth time on each type of substrate (on TiO_2 and on SiO_2). The calculated coverage of the dewet area from microscopic images is shown in Figure 4c. There was no dewet area for both samples of Pt on TiO_2 and SiO_2 at 1.5 min growth time. However, starting with 3 min growth time, Pt thin film on SiO_2 started to show dewetting initiated around the edges of the sample, covering about 15% of the total surface. There was no significant dewet area observed for the Pt thin film on TiO_2. As growth time was increased to 5 min, the surface of Pt thin film on SiO_2 was fully dewet, whereas only 55% of the surface of the Pt thin film on TiO_2 was dewet. At 10 min of growth time, majority of the Pt thin film on TiO_2 was dewet as well. Therefore, microscopic inspection clearly demonstrates that the dewetting is significantly reduced by using the TiO_2 substrate over the SiO_2 substrate when depositing Pt thin film and using it for graphene growth.

https://dx.doi.org/10.1021/acsanm.0c01839
ACS Appl. Nano Mater. 2020, 3, 9731−9739

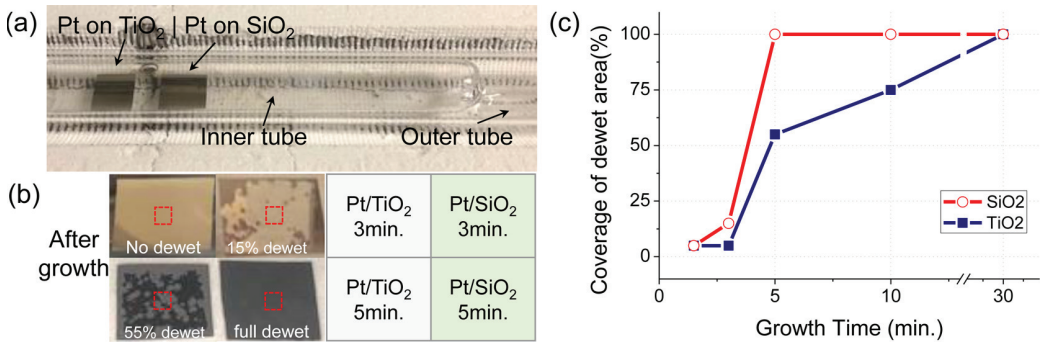

Figure 4. (a) Image of sample loading setup with Pt thin film samples inside the inner tube and (b) comparison between dewetting of Pt on TiO_2 and SiO_2 according to growth time. Growth time of 1.5 min exhibited no significant dewetting surface for both samples. (c) Coverage of the dewet surface area of each sample observed by images according to growth time.

In order to observe more detailed dewetting issues, SEM was used to observe the surface morphology of the Pt thin film at the center of the substrate. Figure 5 shows several SEM images

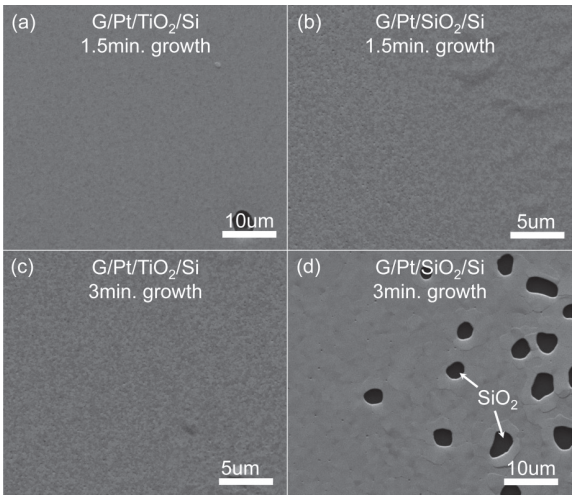

Figure 5. SEM images of Pt deposited on TiO_2 and SiO_2 after graphene growth with different growth times. (a) Pt on the TiO_2 substrate with a growth time of 1.5 min, (b) Pt on the SiO_2 substrate with a growth time of 1.5 min, (c) Pt on the TiO_2 substrate with a growth time of 3 min, and (d) Pt on the SiO_2 substrate with a growth time of 3 min.

of the graphene grown on Pt thin films, either on TiO_2 or on SiO_2 substrates with two different growth times. No significant dewetting was found with both 1.5 min growth substrates, as shown in Figure 5a,b, but starting with 3 min growth, significant dewetting of the Pt thin film surface on the SiO_2 substrate is observable, as shown in Figure 5d, whereas no dewetting is observed on TiO_2, as shown in Figure 5c.

The higher Pt dewetting suppression on TiO_2 compared to Pt on SiO_2 is attributable to the stronger binding between Pt and the TiO_2 layer. We speculate possible reasons from the perspective of surface morphology and adhesion force. Regarding the surface morphology, the root mean square (rms) surface roughness of both SiO_2 and TiO_2 layers has been reported as very small using atomic force microscopy (AFM) (0.4 nm for SiO_2 and less than 2 nm for TiO_2, respectively).[39,44] It is anticipated that the rms roughness of our SiO_2 and TiO_2 layers are comparable to those reported values because we benchmarked processing conditions used in the reference. The small rms roughness of TiO_2 can lead to Pt films with a very smooth surface comparable to that on SiO_2, mainly following the texture of underlying TiO_2 layers.[39] This argument is further supported by the XRD measurement showing {111}-textured Pt film on TiO_2 (see Figure 3 and Table 1). In addition, TiO_2 can have possibly defective sites promoting the strong binding between Pt and TiO_2. However, we have not found noticeable defective sites on both SiO_2 and TiO_2 layers during SEM characterization at high magnification. From the surface morphology perspective, adhesion force between Pt and TiO_2 and SiO_2 layers has been investigated using AFM, where the adhesion force between Pt and the TiO_2 layer is one order of magnitude higher than that on the SiO_2 layer.[44,45] Therefore, Pt dewetting suppression is more observable on Pt/TiO_2/SiO_2 compared to Pt/SiO_2 because of the strong adhesion force between Pt and the TiO_2 layer.

4.3. Effect of Growth Time on Quality of Graphene.

For another quantitative analysis of graphene on Pt thin film (G/Pt), we used TOF-SIMS depth profiling. The overall result of the TOF-SIMS measurement is presented in Figure 6, which shows the yield of a secondary ion fragment of interest, C_9^-, representing graphene, as a function of sputtering time, that is, depth, for both G/Pt/TiO_2 and G/Pt/SiO_2 samples. In the case of the G/Pt/TiO_2 sample, a monolayer-graphene-characteristic depth profile[42,46] is recorded at 1.5 and 3 min growth time, while before growth or at 5 min growth, only some residual C_9^- signal is identified at the surface, which is consistent with highly scattered graphene micropatches (Figure 6a). This implies that graphene that was grown on the surface in the first few minutes of the growth process was totally damaged by dewetting after 5 min of growth time. A similar trend was found on the G/Pt/SiO_2 sample, as shown in Figure 6b. Furthermore, more detailed comparison between G/Pt/TiO_2 and G/Pt/SiO_2 samples uses only the 1.5 and 3 min depth profiles, as shown in Figure 5c. Detailed peak view in the 0−12.5 s of sputter time is presented in Figure 6d, with the inset showing the calculated areas under the depth profiles for comparison. The peak of G/Pt/TiO_2 with 1.5 min growth time has the largest total count of C_9^- secondary ions, indicating that graphene is more uniformly distributed across the surface compared to the other substrates or growth times. With increased growth time to 3 min, the total C_9^- count decreases but remains comparable to the one of 1.5 min growth time. The total C_9^- count for the G/Pt/SiO_2 sample with 1.5 min growth time starts comparable to that of G/Pt/TiO_2 but suffers massive drop within 3 min growth time. As we

https://dx.doi.org/10.1021/acsanm.0c01839
ACS Appl. Nano Mater. 2020, 3, 9731−9739

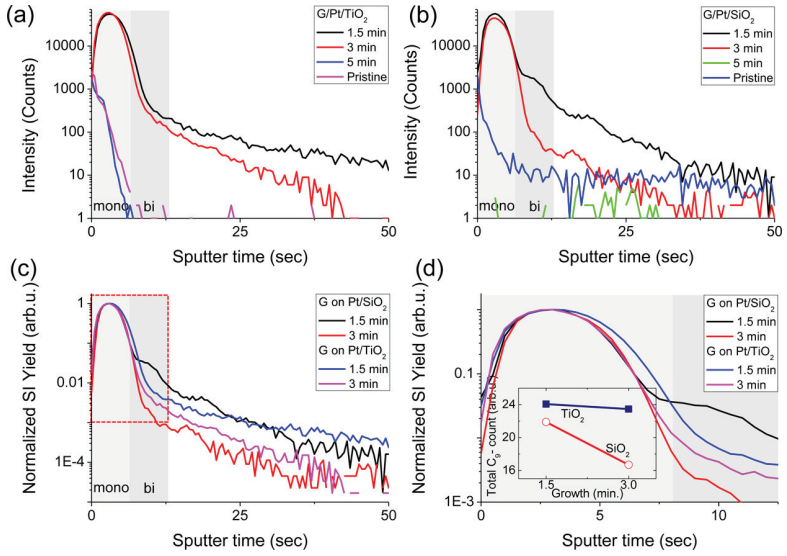

Figure 6. (a) TOF-SIMS depth profiles of a polyatomic carbon fragment, C_9^-, representing graphene for graphene grown on a Pt/TiO_2 substrate with different growth times and (b) on a Pt/SiO_2 substrate. (c) Comparison between the normalized C_9^- depth profiles acquired for graphene grown on Pt/SiO_2 and Pt/TiO_2 substrates with growth times of 1.5 and 3 min. (d) Magnified display of the 0−12.5 s sputtering region showing the mono- and bilayer graphene. The inset shows the total C_9^- count, that is, the depth profiles' areas in the 0−12.5 s sputtering region as function of the substrate and graphene growth time.

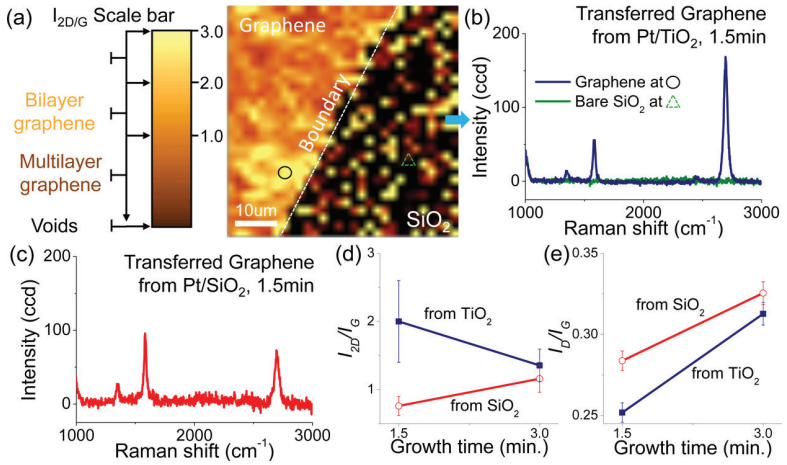

Figure 7. (a) Mapped 2D/G Raman spectrum of graphene transferred from Pt/TiO_2 of 1.5 min growth time and (b) single-point Raman spectrum at each point on graphene and on the transferred substrate of bare SiO_2. (c) Point Raman spectrum of graphene transferred from Pt/SiO_2 of 1.5 min growth time, (d) I_{2D}/I_G ratio according to graphene growth time of 1.5 and 3 min each from Pt/TiO_2 and Pt/SiO_2, and (e) I_D/I_G defect rate ratio according to 1.5 and 3 min each from Pt/TiO_2 and Pt/SiO_2.

observed, significant dewetting starting at 3 min for G/Pt/SiO_2, as shown in Figures 4b and 5d, the TOF-SIMS total C_9^- count result is consistent with lowered coverage of graphene on the surface caused by dewetting of the underlying Pt film. Consequently, we conclude that the remaining graphene region on top of the Pt thin film follows the amount of the surviving Pt thin film surface without dewetting issues.

Although TOF-SIMS measurement relatively quantifies graphene from the readout of carbon counts and depicts the area of remaining graphene region on Pt thin film surface, it does not directly measure the quality of graphene. Therefore, we used Raman spectroscopy to measure the quality of graphene. Graphene grown on each substrate at different growth times was transferred onto separate SiO_2/Si substrates for it to be analyzed by Raman spectroscopy. The Raman mapping of graphene grown on the Pt/TiO_2 substrate is shown in Figure 7a where the color of the scale bar represents the Raman intensity ratio of I_{2D} over I_G. As the ratio of I_{2D}/I_G is closer to 1, graphene is represented as a bilayer, above 1, it is a monolayer, and significantly below 1, it is multilayered.[39] Another way to check approximate number of graphene layers is calculating FWHM of 2D peaks. FWHM of 2D peak in the range of 45−60 cm^{-1} presents bilayered and multilayered graphene, and a FWHM of 20−30 cm^{-1} is monolayered graphene.[47] Graphene from Pt/TiO_2 of 1.5 min growth time shows 28 cm^{-1} of FWHM of 2D peak; hence, it confirms a single layer of graphene. On the other hand, FWHM of 2D peaks from graphene grown from Pt/SiO_2 of 1.5 min growth time is wider of 44 cm^{-1}; hence, more layers than the bilayer graphene are observed. The reason why multiple layers of graphene are favored on Pt/SiO_2 is not clear, but our speculation is that when the unstable Pt thin film has cracks

https://dx.doi.org/10.1021/acsanm.0c01839
ACS Appl. Nano Mater. 2020, 3, 9731−9739

or openings that leads to bottom of the SiO_2 substrate, carbon atoms may reside at the bottom of the Pt thin film, where it forms additional layers of graphene during graphene growth. Pt is known to have low adhesion property on SiO_2 and unstable surface features compared to on TiO_2; hence, it may open up areas for carbon atoms to diffuse down into the bottom of the surface during high-temperature growth. This phenomenon has been reported similarly on the dewet surface of Cu thin film previously where graphene growth occurs on both sides of Cu thin film (the top open surface and the bottom adhesion-layer touching surface).[31]

The Raman spectrum at the location of circle and triangle are represented in Figure 7b which shows clear monolayer graphene on most of graphene-covered region and the bare SiO_2 surface on rest of the surface. On the other hand, graphene is more bilayered on the Pt/SiO_2 substrate, as shown in Figure 7c. In Figure 7d, only monolayered graphene is dominant on the Pt/TiO_2 substrate, and additional layers grow as growth time is increased. This is most likely caused by initial cracks or openings between grain boundaries of the Pt thin film before dewetting of the surface where carbon atoms start to diffuse into the bottom of the Pt thin film and grow another layer below the thin film.[20] As the surface becomes more dewet, more additional layers can grow because of this mechanism. Then, we analyzed the intensity of defected peak at 1347 cm^{-1} (I_D), which shows the presence of defect inherent in the graphene honeycomb lattice.[48] Because each measurement has slightly different noise levels, we have compared I_D to I_G to see how much defect is presen within the samples. According to the I_D/I_G ratios, we conclude that more defect is present in graphene grown on Pt/SiO_2 as compared to graphene on a Pt/TiO_2 substrate, as shown in Figure 7e. This result correlates with the trend of the integrated area of the curve of the C_9^- depth profile (total count) from the TOF-SIMS measurements for each sample. Significant D peak on Pt/SiO_2 with 3 min growth time implies that graphene grown on a heavily dewet substrate is of low quality or has incomplete growth.

Therefore, we believe that growing high-quality monolayer graphene on Pt thin film below 100 nm thickness is feasible by depositing Pt thin film on TiO_2 compared to on SiO_2 as it provides higher thermal stability and favors monolayer growth. Although, graphene integrated devices further require nano-/microfabrication and electrical performance testing for the future application, integration of graphene growth on 100 nm of (111) Pt thin film for NEMS/MEMS device fabrication is more approachable using TiO_2 as the adhesion layer.

5. CONCLUSIONS

In this paper, high-quality graphene growth on Pt thin films with TiO_2 adhesion layers has been demonstrated on Pt thin film of 100 nm thickness. Our Pt thin film is one of the thinnest catalyst layers with a high degree of (111)-Pt orientation reported so far and successfully demonstrated high-quality graphene growth, which enables graphene-integrated devices for NEMS/MEMS applications. In addition, (111)-oriented Pt films were prepared on the TiO_2 and SiO_2 substrate for comparison. TiO_2 was chosen as an adhesion layer for the Pt film to improve Pt adhesion, which, otherwise, would be an obstacle in the Pt film deposited on the SiO_2 substrate. Ti, the most favorable material previously used for Pt film adhesion, has posed diffusion-related issues at high temperature. This is the first-time TiO_2 has been employed as a Pt film adhesion layer for better thermal stability, and in turn, high-quality graphene growth. The direct comparison of Pt film on the TiO_2 substrate against that on the SiO_2 substrate revealed the significant decrease in dewetting of the Pt film during graphene growth while maintaining comparable (111)-Pt crystallization and the graphene quality, which is beneficial for high yield in graphene-integrated device applications.

We conclude that a TiO_2 adhesion layer significantly suppresses the Pt dewetting, leading to high-quality monolayer graphene with less dewet surface. Thermal stability of Pt on TiO_2 is significantly higher than Pt on SiO_2 because of various reasons. One of the main possible reasons is that the adhesion force between Pt on TiO_2 is different from the one from Pt on SiO_2. The adhesion force between Pt on TiO_2 is reported to be several hundred nanonewtons, whereas the adhesion force between Pt on SiO_2 is reported to be 15 nN using AFM measurements.[45,49] Higher adhesion force between the interfaces plays an important role in suppressing dewetting of the Pt thin film. The other possible reason is the different surface morphology of TiO_2 and SiO_2. However, the rms surface roughness for both TiO_2 and SiO_2 layers is reported as less than 2 and 0.4 nm, respectively.[39,44] We believe that both surfaces are smooth enough that the texture of the Pt film is controlled by the texture of the underlying layers, which is supported by our XRD measurement of (111) Pt thin film on the TiO_2 layer.[41] In addition, we have not found noticeable defective sites on both TiO_2 and SiO_2 layers during SEM characterization in high magnification before graphene growth.

■ ASSOCIATED CONTENT

Supporting Information

The Supporting Information is available free of charge at https://pubs.acs.org/doi/10.1021/acsanm.0c01839.

Dewetting properties of Pt at growth temperatures and time, Raman spectrum of graphene grown and transferred from Pt/TiO2 and Pt/SiO2, using C-9 fragment of the TOF-SIMS as the demonstrating marker for single-layer graphene (PDF)

■ AUTHOR INFORMATION

Corresponding Author

Michael A. Cullinan − *Department of Mechanical Engineering, The University of Texas at Austin, Austin, Texas 78712, United States;* orcid.org/0000-0001-8256-7921; Email: michael.cullinan@austin.utexas.edu

Authors

Joon Hyong Cho − *Department of Mechanical Engineering, The University of Texas at Austin, Austin, Texas 78712, United States;* orcid.org/0000-0002-7329-2556

Yoonho Seo − *Department of Electrical and Computer Engineering, The University of Texas at Austin, Austin, Texas 78712, United States;* orcid.org/0000-0001-7503-3323

Andrei Dolocan − *Department of Materials Science and Engineering, The University of Texas at Austin, Austin, Texas 78712, United States;* orcid.org/0000-0001-5653-0439

Neal A. Hall − *Department of Electrical and Computer Engineering, The University of Texas at Austin, Austin, Texas 78712, United States*

Complete contact information is available at: https://pubs.acs.org/10.1021/acsanm.0c01839

https://dx.doi.org/10.1021/acsanm.0c01839
ACS Appl. Nano Mater. 2020, 3, 9731−9739

Author Contributions

[‖]J.H.C. and Y.S. contributed equally to this work.

Notes

The authors declare no competing financial interest.

■ ACKNOWLEDGMENTS

We would like to thank Dr. Alvin Lee, Dr. Richard Piner, and Dr. Deji Akinwande for the helpful discussion on graphene growth on Pt thin film. This research is based upon work supported primarily by the National Science Foundation under cooperative agreement no. EEC-1160494 and by the National Institute of Standards and Technology under grant no. 70NANB19H114.

■ REFERENCES

(1) Bunch, J. S.; van der Zande, A. M.; Verbridge, S. S.; Frank, I. W.; Tanenbaum, D. M.; Parpia, J. M.; Craighead, H. G.; McEuen, P. L. Electromechanical Resonators from Graphene Sheets. *Science* **2007**, *315*, 490−493.

(2) Bolotin, K. I.; Sikes, K. J.; Jiang, Z.; Klima, M.; Fudenberg, G.; Hone, J.; Kim, P.; Stormer, H. L. Ultrahigh Electron Mobility in Suspended Graphene. *Solid State Commun.* **2008**, *146*, 351−355.

(3) Lee, C.; Wei, X.; Kysar, J. W.; Hone, J. Measurement of the Elastic Properties and Intrinsic Strength of Monolayer Graphene. *Science* **2008**, *321*, 385−388.

(4) Pham, V. P.; Jang, H.-S.; Whang, D.; Choi, J.-Y. Direct Growth of Graphene on Rigid and Flexible Substrates: Progress, Applications, and Challenges. *Chem. Soc. Rev.* **2017**, *46*, 6276−6300.

(5) Pham, P. V. Hexagon Flower Quantum Dot-like Cu Pattern Formation during Low-Pressure Chemical Vapor Deposited Graphene Growth on a Liquid Cu/W Substrate. *ACS Omega* **2018**, *3*, 8036−8041.

(6) Seah, C.-M.; Chai, S.-P.; Mohamed, A. R. Mechanisms of Graphene Growth by Chemical Vapour Deposition on Transition Metals. *Carbon* **2014**, *70*, 1−21.

(7) Cho, J. H.; Sun, G.; Cullinan, M. A Method to Manufacture Repeatible Graphene-Based NEMS Devices at the Wafer-Scale. *IEEE J. Sel. Top. Quant. Electron.* **2016**, *17*, 629.

(8) Lin, H.-C.; Chen, Y.-Z.; Wang, Y.-C.; Chueh, Y.-L. The Essential Role of Cu Vapor for the Self-Limit Graphene via the Cu Catalytic CVD Method. *J. Phys. Chem. C* **2015**, *119*, 6835−6842.

(9) Kim, K. S.; Zhao, Y.; Jang, H.; Lee, S. Y.; Kim, J. M.; Kim, K. S.; Ahn, J.-H.; Kim, P.; Choi, J.-Y.; Hong, B. H. Large-Scale Pattern Growth of Graphene Films for Stretchable Transparent Electrodes. *Nature* **2009**, *457*, 706−710.

(10) Pham, V. P.; Nguyen, M. T.; Park, J. W.; Kwak, S. S.; Nguyen, D. H. T.; Mun, M. K.; Phan, H. D.; Kim, D. S.; Kim, K. H.; Lee, N.-E.; Yeom, G. Y. Chlorine-Trapped CVD Bilayer Graphene for Resistive Pressure Sensor with High Detection Limit and High Sensitivity. *2D Mater.* **2017**, *4*, 025049.

(11) Pham, V. P.; Kim, K. N.; Jeon, M. H.; Kim, K. S.; Yeom, G. Y. Cyclic Chlorine Trap-Doping for Transparent, Conductive, Thermally Stable and Damage-Free Graphene. *Nanoscale* **2014**, *6*, 15301−15308.

(12) Kim, S. W.; Seol, M.; Cho, Y.; Shin, K. W.; Lee, D.; Jeong, S.-J.; Lee, H.; Chung, J. G.; Kim, H.-M.; Kim, K.-B.; Park, S.; Shin, H.-J. Graphene-Based Etch Resist for Semiconductor Device Fabrication. *ACS Appl. Nano Mater.* **2020**, *3*, 4635−4641.

(13) Jia, Z.; Zhang, M.; Liu, B.; Wang, F.; Wei, G.; Su, Z. Graphene Foams for Electromagnetic Interference Shielding: A Review. *ACS Appl. Nano Mater.* **2020**, *3*, 6140−6155.

(14) Wang, K.; Li, L.; Zhang, T.; Liu, Z. Nitrogen-Doped Graphene for Supercapacitor with Long-Term Electrochemical Stability. *Energy* **2014**, *70*, 612−617.

(15) Cho, J. H.; Cullinan, M. Graphene Growth on and Transfer From Platinum Thin Films. *J. Micro Nano-Manufacturing* **2017**, *6*, 024501.

(16) Kang, B. J.; Mun, J. H.; Hwang, C. Y.; Cho, B. J. Monolayer Graphene Growth on Sputtered Thin Film Platinum. *J. Appl. Phys.* **2009**, *106*, 104309.

(17) Luo, Z.; Lu, Y.; Singer, D. W.; Berck, M. E.; Somers, L. A.; Goldsmith, B. R.; Johnson, A. T. C. Effect of Substrate Roughness and Feedstock Concentration on Growth of Wafer-Scale Graphene at Atmospheric Pressure. *Chem. Mater.* **2011**, *23*, 1441−1447.

(18) Lee, K.; Ye, J. Significantly Improved Thickness Uniformity of Graphene Monolayers Grown by Chemical Vapor Deposition by Texture and Morphology Control of the Copper Foil Substrate. *Carbon* **2016**, *100*, 441−449.

(19) Thompson, C. V. Solid-State Dewetting of Thin Films. *Annu. Rev. Mater. Res.* **2012**, *42*, 399−434.

(20) Ismach, A.; Druzgalski, C.; Penwell, S.; Schwartzberg, A.; Zheng, M.; Javey, A.; Bokor, J.; Zhang, Y. Direct Chemical Vapor Deposition of Graphene on Dielectric Surfaces. *Nano Lett.* **2010**, *10*, 1542−1548.

(21) Gao, L.; Ren, W.; Xu, H.; Jin, L.; Wang, Z.; Ma, T.; Ma, L.-P.; Zhang, Z.; Fu, Q.; Peng, L.-M.; Bao, X.; Cheng, H.-M. Repeated Growth and Bubbling Transfer of Graphene with Millimetre-Size Single-Crystal Grains Using Platinum. *Nat. Commun.* **2012**, *3*, 699.

(22) Lupina, G.; Kitzmann, J.; Costina, I.; Lukosius, M.; Wenger, C.; Wolff, A.; Vaziri, S.; Östling, M.; Pasternak, I.; Krajewska, A.; Strupinski, W.; Kataria, S.; Gahoi, A.; Lemme, M. C.; Ruhl, G.; Zoth, G.; Luxenhofer, O.; Mehr, W. Residual Metallic Contamination of Transferred Chemical Vapor Deposited Graphene. *ACS Nano* **2015**, *9*, 4776−4785.

(23) Gao, T.; Xie, S.; Gao, Y.; Liu, M.; Chen, Y.; Zhang, Y.; Liu, Z. Growth and Atomic-Scale Characterizations of Graphene on Multi-faceted Textured Pt Foils Prepared by Chemical Vapor Deposition. *ACS Nano* **2011**, *5*, 9194−9201.

(24) Kang, J. H.; Moon, J.; Kim, D. J.; Kim, Y.; Jo, I.; Jeon, C.; Lee, J.; Hong, B. H. Strain Relaxation of Graphene Layers by Cu Surface Roughening. *Nano Lett.* **2016**, *16*, 5993−5998.

(25) Shivaraman, S.; Barton, R. A.; Yu, X.; Alden, J.; Herman, L.; Chandrashekhar, M.; Park, J.; McEuen, P. L.; Parpia, J. M.; Craighead, H. G.; Spencer, M. G. Free-Standing Epitaxial Graphene. *Nano Lett.* **2009**, *9*, 3100−3105.

(26) Sutter, P.; Sadowski, J. T.; Sutter, E. Graphene on Pt(111): Growth and Substrate Interaction. *Phys. Rev. B: Condens. Matter Mater. Phys.* **2009**, *80*, 245411.

(27) Nam, J.; Kim, D.-C.; Yun, H.; Shin, D. H.; Nam, S.; Lee, W. K.; Hwang, J. Y.; Lee, S. W.; Weman, H.; Kim, K. S. Chemical Vapor Deposition of Graphene on Platinum: Growth and Substrate Interaction. *Carbon* **2016**, *111*, 733−740.

(28) Xiao, K.; Wu, H.; Lv, H.; Wu, X.; Qian, H. The Study of the Effects of Cooling Conditions on High Quality Graphene Growth by the APCVD Method. *Nanoscale* **2013**, *5*, 5524−5529.

(29) Liu, L.; Liu, X.; Zhan, Z.; Guo, W.; Xu, C.; Deng, J.; Chakarov, D.; Hyldgaard, P.; Schröder, E.; Yurgens, A.; Sun, J. A Mechanism for Highly Efficient Electrochemical Bubbling Delamination of CVD-Grown Graphene from Metal Substrates. *Adv. Mater. Interfaces* **2016**, *3*, 1500492.

(30) Levendorf, M. P.; Ruiz-Vargas, C. S.; Garg, S.; Park, J. Transfer-Free Batch Fabrication of Single Layer Graphene Transistors. *Nano Lett.* **2009**, *9*, 4479−4483.

(31) Cho, J. H.; Gorman, J. J.; Na, S. R.; Cullinan, M. Growth of Monolayer Graphene on Nanoscale Copper-Nickel Alloy Thin Films. *Carbon* **2017**, *115*, 441−448.

(32) Kweon, S. Y.; Choi, S. K.; Yeom, S. J.; Roh, J. S. Platinum Hillocks in Pt/Ti Film Stacks Deposited on Thermally Oxidized Si Substrate. *Jpn. J. Appl. Phys.* **2001**, *40*, 5850.

(33) Jung, W. W.; Choi, S. K.; Kweon, S. Y.; Yeom, S. J. Platinum(100) Hillock Growth in a Pt/Ti Electrode Stack for Ferroelectric Random Access Memory. *Appl. Phys. Lett.* **2003**, *83*, 2160−2162.

(34) Sreenivas, K.; Reaney, I.; Maeder, T.; Setter, N.; Jagadish, C.; Elliman, R. G. Investigation of Pt/Ti Bilayer Metallization on Silicon

https://dx.doi.org/10.1021/acsanm.0c01839
ACS Appl. Nano Mater. 2020, 3, 9731−9739

for Ferroelectric Thin Film Integration. *J. Appl. Phys.* **1994**, *75*, 232−239.
(35) Fox, G. R.; Trolier-McKinstry, S.; Krupanidhi, S. B.; Casas, L. M. Pt/Ti/SiO2/Si Substrates. *J. Mater. Res.* **1995**, *10*, 1508−1515.
(36) Abe, N.; Otani, Y.; Miyake, M.; Kurita, M.; Takeda, H.; Okamura, S.; Shiosaki, T. Influence of a TiO2Adhesion Layer on the Structure and the Orientation of a Pt Layer in Pt/TiO2/SiO2/Si Structures. *Jpn. J. Appl. Phys.* **2003**, *42*, 2791−2795.
(37) Okamura, S.; Abe, N.; Otani, Y.; Shiosaki, T. Influence of Pt/TiO2 Bottom Electrodes on the Properties of Ferroelectric Pb-(Zr,Ti)O3 Thin Films. *Integr. Ferroelectr.* **2003**, *52*, 127−136.
(38) Sanchez, L. M.; Potrepka, D. M.; Fox, G. R.; Takeuchi, I.; Wang, K.; Bendersky, L. A.; Polcawich, R. G. Optimization of PbTiO3 Seed Layers and Pt Metallization for PZT-Based PiezoMEMS Actuators. *J. Mater. Res.* **2013**, *28*, 1920−1931.
(39) Fox, A. J.; Drawl, B.; Fox, G. R.; Gibbons, B. J.; Trolier-McKinstry, S. Control of Crystallographic Texture and Surface Morphology of Pt/Tio2 Templates for Enhanced PZT Thin Film Texture. *IEEE Trans. Ultrason. Ferroelectr. Freq. Control* **2015**, *62*, 56−61.
(40) Srolovitz, D. J.; Safran, S. A. Capillary Instabilities in Thin Films. 2: Kinetics. *J. Appl. Phys.* **1986**, *247*, 255−260.
(41) Fox, G. R.; Potrepka, D. M.; Polcawich, R. G. Dependence of {111}-Textured Pt Electrode Properties on TiO2 Seed Layers Formed by Thermal Oxidation. *J. Mater. Sci. Mater. Electron.* **2018**, *29*, 412−426.
(42) Chou, H.; Ismach, A.; Ghosh, R.; Ruoff, R. S.; Dolocan, A. Revealing the Planar Chemistry of Two-Dimensional Heterostructures at the Atomic Level. *Nat. Commun.* **2015**, *6*, 7482.
(43) Griffin, M. P.; Gearba, R.; Stevenson, K. J.; Vanden Bout, D. A.; Dolocan, A. Revealing the Chemistry and Morphology of Buried Donor/Acceptor Interfaces in Organic Photovoltaics. *J. Phys. Chem. Lett.* **2017**, *8*, 2764−2773.
(44) Zúñiga-Segundo, A.; Ruiz, F.; Vázquez-López, C.; González-Hernández, J.; Torres-Delgado, G.; Tsu, D. V. Characterization of SiO2 Layers on Si Wafers Using Atomic Force Microscopy. *J. Vac. Sci. Technol., A* **1994**, *12*, 2572−2576.
(45) Moon, H.; Zade, V.; Kang, H.-S.; Han, J.-W.; Lee, E.; Hwang, C. S.; Lee, M. H. Interfacial Chemical Bonding-Mediated Ionic Resistive Switching. *Sci. Rep.* **2017**, *7*, 1264.
(46) Wang, X.; Dolocan, A.; Chou, H.; Tao, L.; Dick, A.; Akinwande, D.; Willson, C. G. Direct Observation of Poly(Methyl Methacrylate) Removal from a Graphene Surface. *Chem. Mater.* **2017**, *29*, 2033−2039.
(47) Cho, J. H.; Na, S. R.; Park, S.; Akinwande, D.; Liechti, K. M.; Cullinan, M. A. Controlling the Number of Layers in Graphene Using the Growth Pressure. *Nanotechnology* **2019**, *30*, 235602.
(48) Lucchese, M. M.; Stavale, F.; Ferreira, E. H. M.; Vilani, C.; Moutinho, M. V. O.; Capaz, R. B.; Achete, C. A.; Jorio, A. Quantifying Ion-Induced Defects and Raman Relaxation Length in Graphene. *Carbon* **2010**, *48*, 1592−1597.
(49) Eppler, A. S.; Rupprechter, G.; Anderson, E. A.; Somorjai, G. A. Thermal and Chemical Stability and Adhesion Strength of Pt Nanoparticle Arrays Supported on Silica Studied by Transmission Electron Microscopy and Atomic Force Microscopy. *J. Phys. Chem. B* **2000**, *104*, 7286−7292.

https://dx.doi.org/10.1021/acsanm.0c01839
ACS Appl. Nano Mater. 2020, 3, 9731−9739